

# Estimation of ordinary differential equation models with discretization error quantification

Takeru Matsuda\* and Yuto Miyatake†

**Abstract.** We consider estimation of ordinary differential equation (ODE) models from noisy observations. For this problem, one conventional approach is to fit numerical solutions (e.g., Euler, Runge–Kutta) of ODEs to data. However, such a method does not account for the discretization error in numerical solutions and has limited estimation accuracy. In this study, we develop an estimation method that quantifies the discretization error based on data. The key idea is to model the discretization error as random variables and estimate their variance simultaneously with the ODE parameter. The proposed method has the form of iteratively reweighted least squares, where the discretization error variance is updated with the isotonic regression algorithm and the ODE parameter is updated by solving a weighted least squares problem using the adjoint system. Experimental results demonstrate that the proposed method improves estimation accuracy by accounting for the discretization error in a data-driven manner.

**Key words.** discretization error, parameter estimation, uncertainty quantification

**AMS subject classifications.** 62F10, 65L05

**1. Introduction.** A system of ordinary differential equations (ODEs) is a fundamental tool for modeling a dynamical system in many fields. For example, the spiking neuron activity is simply described by the FitzHugh–Nagumo model:

$$\frac{dV}{dt} = c \left( V - \frac{V^3}{3} + R \right), \quad \frac{dR}{dt} = -\frac{1}{c}(V - a + bR).$$

In practice, ODE models often include unknown system parameters (e.g.,  $a$ ,  $b$ , and  $c$  in the above model) or unknown initial state (e.g.,  $V(0)$  and  $R(0)$  in the above model). In this study, we focus on estimation of ODE models from noisy data. Specifically, consider an ODE model

$$\frac{d}{dt}x(t; \theta) = f(x(t; \theta), \theta), \quad x(0; \theta) = x_0(\theta),$$

where  $\theta \in \Theta \subset \mathbb{R}^D$  is an unknown parameter. Suppose that we have noisy observations  $y_1, \dots, y_K$  of  $x(t; \theta)$  at several time points  $t_1, \dots, t_K$ :

$$(1.1) \quad y_k = Hx(t_k; \theta) + \varepsilon_k, \quad \varepsilon_k \sim N(0, \Gamma), \quad k = 1, \dots, K,$$

where  $H$  is a given linear map and  $\varepsilon_k$  is the observation noise with covariance  $\Gamma$ . In this setting, our goal is to estimate  $\theta$  based on  $y_1, \dots, y_K$ .

---

\*Department of Mathematical Informatics, Graduate School of Information Science and Technology, The University of Tokyo, Japan; Mathematical Informatics Collaboration Unit, RIKEN Center for Brain Science, Japan ([matsuda@mist.i.u-tokyo.ac.jp](mailto:matsuda@mist.i.u-tokyo.ac.jp))

†Cybermedia Center, Osaka University, Japan ([miyatake@cas.cmc.osaka-uac.jp](mailto:miyatake@cas.cmc.osaka-uac.jp)).

Estimation of ODE models has a distinct feature due to the intractability of the initial value problems. Namely, ODEs do not have a closed-form solution in general, and thus, we do not have access to the exact solution  $x(t_k; \theta)$  in (1.1). In this sense, our problem here is essentially different from the usual nonlinear regression. Instead of the exact solution  $x(t_k; \theta)$ , its approximation  $\tilde{x}(t_k; \theta)$  is obtained by using numerical methods for ODEs such as Euler and Runge–Kutta [5, 13]. Thus, one simple conventional approach to parameter estimation in ODE models is to fit the numerical solutions to data directly. However, this approach requires numerical solutions to be sufficiently accurate, which is computationally intensive in general. In other words, the difference  $\tilde{x}(t_k; \theta) - x(t_k; \theta)$  between the numerical and exact solutions, which we call the discretization error in the following, is not negligible.

In this study, we develop a method for estimating ODE models that quantifies the discretization error based on data. The key idea is to model the discretization error as random variables, which is inspired from the recent studies on probabilistic numerics for differential equations [8, 15, 18], and estimate their variance simultaneously with the ODE parameter. Specifically, the proposed method has the form of Iteratively Reweighted Least Squares (IRLS), where the discretization error variance and ODE parameter are alternately updated. The update of the discretization error variance is efficiently solved by the isotonic regression algorithm [3, 22, 30]. On the other hand, the update of the ODE parameter is formulated as a weighted least squares problem and solved by using the exact gradient of an objective function, which is computed by the adjoint system of (1.1) and symplectic partitioned Runge–Kutta methods [24]. Experimental results on several ODE models demonstrate that the proposed method successfully quantifies the discretization error and thus has better estimation accuracy than the conventional method. Note that, whereas several recent studies investigated Bayesian probabilistic numerical methods for ODE models [6, 7, 21], we focus on parameter estimation with maximum likelihood in this study.

This paper is organized as follows. After presenting the problem setting in Section 2, we explain the detail of the proposed method in Section 3. In Section 4, we show the experimental results for several ODE models. In Section 5, we give concluding remarks. Several technical details are provided in the appendices.

**2. Problem setting.** Consider an  $M$ -dimensional ODE model

$$(2.1) \quad \frac{d}{dt}x(t; \theta) = f(x(t; \theta), \theta), \quad x(0; \theta) = x_0(\theta),$$

where  $f : \mathbb{R}^M \times \mathbb{R}^D \rightarrow \mathbb{R}^M$  and  $\theta \in \Theta \subset \mathbb{R}^D$  is an unknown parameter. Suppose that we have noisy observations  $y_1, \dots, y_K$  of  $J$  ( $\leq M$ ) components of  $x(t; \theta)$  at  $K$  time points  $0 \leq t_1 < t_2 < \dots < t_K$ :

$$(2.2) \quad y_k = Hx_k(\theta) + \varepsilon_k, \quad \varepsilon_k \sim N(0, \Gamma), \quad k = 1, \dots, K,$$

where  $H \in \mathbb{R}^{J \times M}$  is a submatrix of the identity matrix of size  $M$ ,  $x_k(\theta) := x(t_k; \theta)$  is the exact solution of (2.1) at  $t = t_k$ , and  $\varepsilon_1, \dots, \varepsilon_K$  are i.i.d. observation noise. For simplicity, we assume the covariance matrix  $\Gamma$  of the observation noise  $\varepsilon_k$  to be a known diagonal matrix:  $\Gamma = \text{diag}(\gamma_1^2, \dots, \gamma_J^2)$  with  $\gamma_j^2 > 0$  given. We denote the  $j$ -th element of  $y_k$  and  $Hx_k$  by  $y_{k,j}$  and  $H_jx_k$ , respectively, for  $j = 1, \dots, J$ .

Our goal is to estimate  $\theta$  based on  $y_1, \dots, y_K$ . From (2.2), the likelihood function is given by

$$L(\theta) = p(y_1, \dots, y_K \mid \theta) = \prod_{k=1}^K \frac{1}{(2\pi)^{J/2} |\Gamma|^{1/2}} \exp\left(-\frac{1}{2}(y_k - Hx_k(\theta))^\top \Gamma^{-1}(y_k - Hx_k(\theta))\right).$$

Therefore, the maximum likelihood (ML) estimate is the solution of the least squares problem:

$$(2.3) \quad \hat{\theta}_{\text{ML}} = \underset{\theta}{\operatorname{argmax}} \log L(\theta) = \underset{\theta}{\operatorname{argmin}} \sum_{k=1}^K (y_k - Hx_k(\theta))^\top \Gamma^{-1}(y_k - Hx_k(\theta)).$$

Although the maximum likelihood estimate  $\hat{\theta}_{\text{ML}}$  in (2.3) has desirable properties including asymptotic efficiency, it involves the exact solution  $x_k(\theta)$  of the ODE model (2.1), which is not available in practice. Thus, one conventional method is to substitute a numerical solution  $\tilde{x}_k(\theta)$  such as Euler and Runge–Kutta [5, 13], which we call the quasi-maximum likelihood (QML) estimate:

$$(2.4) \quad \hat{\theta}_{\text{QML}} = \underset{\theta}{\operatorname{argmin}} \sum_{k=1}^K (y_k - H\tilde{x}_k(\theta))^\top \Gamma^{-1}(y_k - H\tilde{x}_k(\theta)).$$

If the numerical solution  $\tilde{x}_k(\theta)$  is sufficiently accurate, then the estimate  $\hat{\theta}_{\text{QML}}$  in (2.4) is considered to be close to the maximum likelihood estimate (2.3). However, the discretization error  $\tilde{x}_k(\theta) - x_k(\theta)$  is not negligible in general, and thus, the estimate  $\hat{\theta}_{\text{QML}}$  in (2.4) has limited estimation accuracy. We give one simple example in the following.

*Example 2.1.* Consider initial value estimation in the one-dimensional linear ODE model:

$$\frac{d}{dt}x(t; \theta) = \lambda x(t; \theta), \quad x(0; \theta) = \theta,$$

with observations

$$y_k = x(t_k; \theta) + r_k, \quad r_k \sim \mathcal{N}(0, \gamma^2), \quad k = 1, \dots, K,$$

where  $\lambda > 0$  and  $t_k = kh$ . This ODE model has the closed-form solution given by

$$x_k(\theta) = \exp(\lambda kh)\theta.$$

On the other hand, if we solve this ODE with the explicit Euler scheme with step size  $h$ , then the numerical solution is given by

$$\tilde{x}_k(\theta) = (1 + \lambda h)^k \theta.$$

Thus, if we adopt this numerical solution, the quasi-maximum likelihood estimate of  $\theta$  in (2.4) is given by

$$\hat{\theta}_{\text{QML}} = \underset{\theta}{\operatorname{argmin}} \sum_{k=1}^K (y_k - (1 + \lambda h)^k \theta)^2.$$

This estimator is biased, and its bias is calculated as

$$\mathbb{E}_\theta[\hat{\theta}_{\text{QML}}] - \theta = \frac{\sum_{k=1}^K \exp(\lambda k h)(1 + \lambda h)^k}{\sum_{k=1}^K (1 + \lambda h)^{2k}},$$

which diverges as  $K \rightarrow \infty$ .

**3. Proposed method.** In this section, we develop a method for parameter estimation in ODE models (2.1) that quantifies the discretization error in a data-driven manner. In Section 3.1, we introduce the main idea of modeling the discretization error as random variables and formulate the problem to simultaneous estimation of the discretization error variance and ODE parameter. In Section 3.2, we propose Iteratively Reweighted Least Squares (IRLS) algorithms where the discretization error variance and ODE parameter are alternately updated. The update schemes for the discretization error variance and the ODE parameter are explained in Sections 3.3 and 3.4, respectively.

**3.1. Discretization error as random variable.** Let  $\xi_k := \tilde{x}_k - x_k$  be the discretization error at  $k$ -th step. We model  $\xi_1, \dots, \xi_K$  as independent Gaussian random variables:

$$(3.1) \quad \xi_k \sim \mathcal{N}(0, V_k), \quad k = 1, \dots, K,$$

where the variance  $V_k = \text{diag}(v_{k,1}, \dots, v_{k,J})$  quantifies the magnitude of  $\xi_k$ . Since the discretization error is considered to accumulate in every step of numerical integration, we assume the discretization error variances to be non-decreasing:

$$(3.2) \quad 0 \leq v_{1,j} \leq v_{2,j} \leq \dots \leq v_{K,j}, \quad j = 1, \dots, J.$$

By substituting (3.1) into (2.2), we obtain

$$(3.3) \quad y_k = H\tilde{x}_k(\theta) + e_k, \quad e_k \sim \mathcal{N}(0, \Gamma + \Sigma_k), \quad k = 1, \dots, K,$$

where  $e_k := -H\xi_k + \varepsilon_k$  and  $\Sigma_k := HV_kH^\top$ . Note that we used the independence of the discretization error  $\xi_1, \dots, \xi_K$  and the observation noise  $\varepsilon_1, \dots, \varepsilon_K$ . Since  $H \in \mathbb{R}^{J \times M}$  is a submatrix of the identity matrix of size  $M$  and  $V_k$  has the order constraint (3.2), we have

$$\Sigma_k = \text{diag}(\sigma_{k,1}^2, \dots, \sigma_{k,J}^2), \quad k = 1, \dots, K,$$

where

$$(3.4) \quad 0 \leq \sigma_{1,j}^2 \leq \sigma_{2,j}^2 \leq \dots \leq \sigma_{K,j}^2, \quad j = 1, \dots, J.$$

We estimate the discretization error variance  $\Sigma := (\Sigma_1, \dots, \Sigma_K)$  simultaneously with the ODE parameter  $\theta$  by maximum likelihood. From (3.3), the likelihood function is given by

$$\begin{aligned} L(\theta, \Sigma) &= p(y_1, \dots, y_K \mid \theta, \Sigma) \\ &= \prod_{k=1}^K \frac{1}{(2\pi)^{J/2} |\Gamma + \Sigma_k|^{1/2}} \exp\left(-\frac{1}{2}(y_k - H\tilde{x}_k(\theta))^\top (\Gamma + \Sigma_k)^{-1} (y_k - H\tilde{x}_k(\theta))\right). \end{aligned}$$

Thus, the estimate is defined as

$$\begin{aligned}
 (\hat{\theta}, \hat{\Sigma}) &= \operatorname{argmax}_{\theta, \Sigma} \log L(\theta, \Sigma) \\
 &= \operatorname{argmin}_{\theta, \Sigma} \sum_{k=1}^K \left( \log |\Gamma + \Sigma_k| + (y_k - H\tilde{x}_k(\theta))^\top (\Gamma + \Sigma_k)^{-1} (y_k - H\tilde{x}_k(\theta)) \right) \\
 (3.5) \quad &= \operatorname{argmin}_{\theta, \Sigma} \sum_{k=1}^K \sum_{j=1}^J \left( \log(\gamma_j^2 + \sigma_{k,j}^2) + \frac{r_{k,j}^2(\theta)}{\gamma_j^2 + \sigma_{k,j}^2} \right),
 \end{aligned}$$

where  $r_{k,j}(\theta)$  is the residual defined by

$$(3.6) \quad r_{k,j}(\theta) = y_{k,j} - H_j \tilde{x}_k(\theta).$$

*Remark 3.1.* The idea of modeling the discretization error by random variables was discussed recently by, for example, Arnold et al. [2] and Conrad et al. [8]. In [8], by modeling the local truncation error by Gaussian random variables, the authors proposed to quantify the forward uncertainty by doing a number of simulations and applied this method to improve the Bayesian inference. Convergence analyses are given in [18]. To preserve properties such as positivity and symplecticity, Abdulle and Garegnani [1] proposed to perturb the time step size instead. On the other hand, several studies have investigated the relationship between ODE solvers and Gaussian process models [26, 27, 28] and its implications for uncertainty quantification [6, 16, 14, 27, 29]. We also note that probabilistic models have been used in the context of numerical analysis, see, e.g., Hairer et al. [12].

**3.2. Iteratively reweighted least squares.** Now, we develop Iteratively Reweighted Least Squares (IRLS) algorithms for solving (3.5).

We introduce the weights  $w = (w_{k,j})$  defined by

$$w_{k,j} = \frac{1}{\gamma_j^2 + \sigma_{k,j}^2}, \quad k = 1, \dots, K, \quad j = 1, \dots, J.$$

From (3.4), the weights have the order constraint:

$$(3.7) \quad 0 < w_{K,j} \leq w_{K-1,j} \leq \dots \leq w_{1,j} \leq \frac{1}{\gamma_j^2}, \quad j = 1, \dots, J.$$

By transforming from  $(\theta, \Sigma)$  to  $(\theta, w)$ , the minimization problem in (3.5) is rewritten as

$$(3.8) \quad (\hat{\theta}, \hat{w}) = \operatorname{argmin}_{\theta, w} g(\theta, w),$$

where

$$(3.9) \quad g(\theta, w) = \sum_{k=1}^K \sum_{j=1}^J (-\log w_{k,j} + w_{k,j} r_{k,j}^2(\theta)).$$

We solve (3.8) by alternating minimization with respect to  $\theta$  and  $w$ . Specifically, starting from an initial guess  $\theta^{(0)}$  of the ODE parameter, we iterate the following two steps:

$$(3.10) \quad w^{(l)} = \underset{w}{\operatorname{argmin}} g(\theta^{(l-1)}, w),$$

$$(3.11) \quad \theta^{(l)} = \underset{\theta}{\operatorname{argmin}} g(\theta, w^{(l)}).$$

The detail of each update will be explained in the following two subsections. Since the update of  $\theta$  in (3.11) is interpreted as a weighted least squares with weights  $w$ , we refer to the algorithm that iterates (3.10) and (3.11) until convergence as the Iteratively Reweighted Least Squares (IRLS) algorithm (Algorithm 3.1). In addition, we call  $L$  iterations of (3.10) and (3.11) the IRLS( $L$ ) algorithm (Algorithm 3.2). From the order constraint (3.7), the estimated weights  $\hat{w}_{k,j}$  are non-increasing with respect to  $k$  and they are interpreted as describing the reliability of the numerical solution  $\tilde{x}_{k,j}(\theta)$  in estimating  $\theta$ .

---

**Algorithm 3.1** Iteratively reweighted least squares (IRLS) for solving (3.8)

---

- 1: Set the initial guess  $\theta^{(0)}$
  - 2: **for**  $l = 1, 2, \dots$  **do**
  - 3:   Solve (3.10) by PAVA (Section 3.3)
  - 4:   Solve (3.11) by numerical optimization (Section 3.4)
  - 5:   **if** stopping criterion is satisfied **then**
  - 6:     Return  $w^{(l)}$  and  $\theta^{(l)}$
  - 7:   **end if**
  - 8: **end for**
- 

---

**Algorithm 3.2** Iteratively reweighted least squares ( $L$ ) (IRLS( $L$ )) for solving (3.8)

---

- 1: Set the initial guess  $\theta^{(0)}$
  - 2: **for**  $l = 1, 2, \dots, L$  **do**
  - 3:   Solve (3.10) by PAVA (Section 3.3)
  - 4:   Solve (3.11) by numerical optimization (Section 3.4)
  - 5: **end for**
  - 6: Return  $w^{(L)}$  and  $\theta^{(L)}$
- 

**3.3. Update of the weights.** Here, we provide an efficient method for the update of the weights  $w$  in (3.10).

The update of the weights (3.10) is solved as follows. Its proof is given in Appendix A.

**Theorem 3.2.** *Let  $(\mu_{1,j}, \dots, \mu_{K,j})$  be the optimal solution of*

$$(3.12) \quad \min_{\mu_{1,j} \leq \dots \leq \mu_{K,j} < 0} \sum_{k=1}^K \left( \Phi(\mu_{k,j}) - \mu_{k,j} r_{k,j}(\theta^{(l-1)})^2 \right),$$

where  $\Phi(\mu) = -\log(-\mu)$ , for  $j = 1, \dots, J$ . Then, the solution of (3.10) is given by  $w_{k,j}^{(l)} = -\max(\mu_{k,j}, -1/\gamma_j^2)$  for  $j = 1, \dots, J$ .

The optimization problem (3.12) is efficiently solved by an algorithm called the pool adjacent violators algorithm (PAVA) [3, 22, 30]. Specifically, let  $S_0 = 0$  and  $S_k = r_{1,j}^2 + \dots + r_{k,j}^2$  for  $k = 1, \dots, K$ . Consider the line graph connecting  $(0, S_0), (1, S_1), \dots, (K, S_K)$  (dashed line in Figure 3.1). We can efficiently compute the maximal convex function, called the greatest convex minorant, on  $[0, K]$  which lies entirely below this graph (solid line in Figure 3.1). Let  $\bar{S}_k$  be the value of the greatest convex minorant at  $k$  for  $k = 0, 1, \dots, K$ . Then, the optimal solution to (3.12) is given by

$$\hat{\mu}_k = \phi^{-1}(\bar{S}_k - \bar{S}_{k-1}) = -\frac{1}{\bar{S}_k - \bar{S}_{k-1}}, \quad k = 1, \dots, K,$$

where  $\phi(\mu) = \Phi'(\mu) = -1/\mu$ . See [22] for the proof.

The computational cost for updating the weights is much cheaper than that for a single numerical integration of the system of ODEs (2.1) in most cases. Note also that the weights  $w = (w_{k,j})$  for different  $j$  can be updated in parallel.

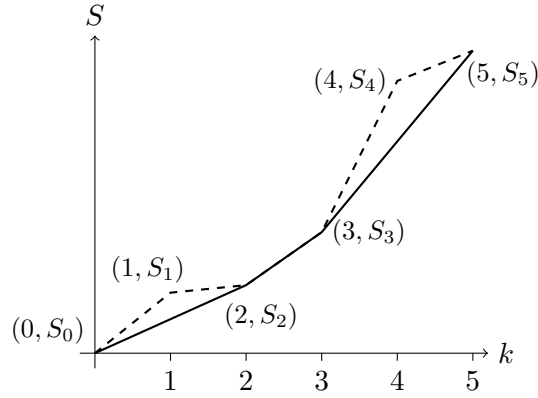


**Figure 3.1.** The line graph with  $K = 5$  (dashed line) and its greatest convex minorant (solid line).

**Remark 3.3.** PAVA is a general algorithm for the problem of estimating ordered natural parameters of exponential families, which is called the generalized isotonic regression [3, 22, 30], and the update of the weights is naturally interpreted in this context. Namely, from (3.3), the square of the residual (3.6) follows the chi-square distribution:

$$r_{k,j}(\theta)^2 \sim (\gamma_j^2 + \sigma_{k,j}^2) \chi_1^2.$$

In other words,  $r_{k,j}(\theta)^2$  follows the Gamma distribution with shape parameter  $1/2$  and scale parameter  $w_{k,j}^{-1} = \gamma_j^2 + \sigma_{k,j}^2$ :

$$r_{k,j}(\theta)^2 \sim \text{Gamma}\left(\frac{1}{2}, \frac{1}{w_{k,j}}\right).$$

In this way, the procedure above can be interpreted as applying PAVA to the maximum likelihood estimation of ordered scale parameters of Gamma distributions (see Example 1.5.3 in [22]).

**3.4. Update of the ODE parameter.** The update of the ODE parameter  $\theta$  in (3.11) is interpreted as solving the weighted least squares problem:

$$(3.13) \quad \theta^{(l)} = \underset{\theta}{\operatorname{argmin}} \tilde{R}(\theta),$$

where

$$(3.14) \quad \tilde{R}(\theta) = \sum_{k=1}^K \tilde{R}_k(\theta), \quad \tilde{R}_k(\theta) = \sum_{j=1}^J w_{k,j}^{(l)} (y_{k,j} - H_j \tilde{x}_k(\theta))^2.$$

We employ numerical optimization to solve (3.13). In order to use a gradient method such as the quasi-Newton method and nonlinear conjugate gradient method, the gradient  $\nabla_{\theta} \tilde{R}(\theta)$  of the objective function  $\tilde{R}(\theta)$  is necessary. However, since the objective function  $\tilde{R}(\theta)$  is implicitly defined through the ODE solver  $\tilde{x}_k(\theta)$ , computation of its gradient is not trivial. In this subsection, we briefly review a method for efficiently computing the gradient of  $\tilde{R}(\theta)$ . The key ingredients are the adjoint system and symplectic partitioned Runge–Kutta scheme [23]. See [24] for more detail.

Let us focus on an  $M$ -dimensional ODE model with unknown initial state:

$$(3.15) \quad \frac{d}{dt}x(t; \theta) = f(x(t; \theta)), \quad x(0; \theta) = \theta.$$

The adjoint system of (3.15) is defined as

$$(3.16) \quad \frac{d}{dt}\lambda(t) = -\nabla_x f(x(t; \theta))^{\top} \lambda(t),$$

where  $\lambda(t) \in \mathbb{R}^M$  and  $\nabla_x f(x(t; \theta))$  denotes the Jacobian matrix of  $f$  at  $z(x(t; \theta))$ . For a function of the form  $R(\theta) = J(x(T; \theta))$ , the backward solution of the adjoint system (3.16) with the final state condition  $\lambda(T) = \nabla_x J(x(T; \theta))$  satisfies  $\lambda(0) = \nabla_{\theta} R(\theta)$  (see Proposition 3.1 in [24]). Similar relation holds when the original system (3.15) and adjoint system (3.16) are discretized by a symplectic partitioned Runge–Kutta scheme [23], which is a well-known scheme in the context of *Geometric Integration* [11, 25] (see Appendix B for a brief introduction of geometric integration and symplectic partitioned Runge–Kutta methods). Specifically, let  $\tilde{x}_k(\theta)$  and  $\tilde{\lambda}_k$  be the numerical solution of (3.15) and (3.16) by a symplectic partitioned Runge–Kutta scheme. Then, for a function of the form  $\tilde{R}(\theta) = J(\tilde{x}_K(\theta))$ , the backward solution of the adjoint system (3.16) with the final state condition  $\tilde{\lambda}_K = \nabla_x J(\tilde{x}_K(\theta))$  satisfies  $\tilde{\lambda}_0 = \nabla_{\theta} \tilde{R}(\theta)$  (see Theorem 3.4 in [24]). For example, if the ODE model (3.15) is discretized by the explicit Euler scheme

$$(3.17) \quad \frac{\tilde{x}_{k+1}(\theta) - \tilde{x}_k(\theta)}{t_{k+1} - t_k} = f(\tilde{x}_k(\theta)),$$

then the adjoint system (3.16) should be discretized as

$$(3.18) \quad \frac{\tilde{\lambda}_{k+1} - \tilde{\lambda}_k}{t_{k+1} - t_k} = -\nabla_x f(\tilde{x}_k(\theta))^{\top} \tilde{\lambda}_{k+1},$$



which is an explicit scheme for backward integration.

The objective function  $\tilde{R}(\theta)$  in (3.13) is a sum of  $\tilde{R}_k(\theta)$  in (3.14). Therefore, when we adopt the explicit Euler method (3.17) for the numerical solution  $\tilde{x}_k$ , the procedure of computing the gradient of  $\tilde{R}(\theta)$  is given by Algorithm 3.3. Its output  $\tilde{\lambda}_0$  coincides with  $\nabla_{\theta}\tilde{R}(\theta)$ . Of course, this procedure can be extended straightforwardly to more general Runge–Kutta schemes. In Section 4.3, we will use the Störmer–Verlet method (see Appendix C) for the numerical solution of the Kepler equation. Also note that, in practice, we can adopt a composition of Runge–Kutta schemes with time step sizes smaller than the observation interval  $t_{k+1} - t_k$ , as will be done in Section 4.

---

**Algorithm 3.3** Exact calculation of the gradient  $\nabla_{\theta}\tilde{R}(\theta)$  of  $\tilde{R}(\theta)$  in (3.14)

---

- 1: Compute the numerical solutions  $\tilde{x}_1, \dots, \tilde{x}_K$  for (3.15) using the Euler method (3.17)
  - 2: Set  $\tilde{\lambda}_K = \nabla_x R_K(\tilde{x}_K(\theta))$
  - 3: **for**  $k = 1, \dots, K$  **do**
  - 4:   Calculate  $\tilde{\lambda}_{K-k}$  using (3.18)
  - 5:   **if**  $k = K$  **then**
  - 6:     Return  $\tilde{\lambda}_0$
  - 7:   **end if**
  - 8:    $\tilde{\lambda}_{K-k} \leftarrow \tilde{\lambda}_{K-k} + \nabla_x R_{K-k}(\tilde{x}_{K-k}(\theta))$
  - 9: **end for**
- 

Although we focused on the ODE model with unknown initial state (3.15), the above method is applicable to the ODE model (2.1) with unknown system parameter as well. Specifically, if the ODE model (2.1) includes the unknown system parameter  $\theta_S$ , then it is reduced to the form of (3.15) as follows:

$$\frac{d}{dt} \begin{bmatrix} x(t; \theta) \\ u(t; \theta) \end{bmatrix} = \begin{bmatrix} f(x(t; \theta)) \\ 0 \end{bmatrix}, \quad \begin{bmatrix} x(0; \theta) \\ u(0; \theta) \end{bmatrix} = \begin{bmatrix} x_0(\theta) \\ \theta_S \end{bmatrix}.$$

Thus, the above method efficiently computes the gradient of  $\tilde{R}(\theta)$  in (3.14).

**4. Numerical experiments.** In this section, we investigate the performance of the IRLS algorithms by numerical experiments on three ODE models: Lorenz system, FitzHugh–Nagumo model and Kepler equation. Experiments were performed in a computation environment with 1.6 GHz Intel Core i5, 16 GB memory, Mac OS X 10.14.4, and MATLAB (R2019a).

In each experiment, we generated observation data  $y_1, \dots, y_K$  by solving the ODE model (2.1) with the MATLAB function `ode45` and then adding Gaussian observation noise following (2.2). In `ode45`, both relative and absolute error tolerances were set to  $3.0 \times 10^{-14}$ , which is much smaller than the observation noise variance employed below.

For the Lorenz system and FitzHugh–Nagumo model, we employed the explicit Euler method for the numerical solution  $\tilde{x}(t; \theta)$ . On the other hand, for the Kepler equation, we used the Störmer–Verlet method, which is a symplectic integrator for Hamiltonian systems [11] (see Appendix C). Note that the time step size was set to be smaller than the observation interval in all cases.

To solve the weighted least squares in (3.11), we used the MATLAB function `fminunc` (quasi-Newton algorithm; BFGS) with the gradient computed by the method in Section 3.4. We have also tested `fminunc` (trust-region algorithm) and the nonlinear conjugate gradient method, but the quasi-Newton algorithm was the fastest in many cases.

As shown in Figure 4.1, the IRLS algorithms converged within a few iterations in most cases. Thus, instead of providing a specific stopping criterion for IRLS (Algorithm 3.1), we simply identify IRLS(20) (Algorithm 3.2) as IRLS (Algorithm 3.1).

**4.1. Lorenz system.** Here, we consider the Lorenz system [19]:

$$\frac{d}{dt} \begin{bmatrix} x_1 \\ x_2 \\ x_3 \end{bmatrix} = \begin{bmatrix} \sigma(-x_1 + x_2) \\ x_1(\rho - x_3) - x_2 \\ x_1x_2 - \beta x_3 \end{bmatrix}, \quad \begin{bmatrix} x_1(0) \\ x_2(0) \\ x_3(0) \end{bmatrix} = \theta,$$

where  $(\sigma, \rho, \beta) = (10, 28, 8/3)$ .

We focus on estimation of the initial state  $\theta = [-10, -1, 40]^\top$  from the observation of  $(x_1, x_2, x_3)$ . Namely, the observation matrix  $H$  in (2.2) is the identity matrix. The observation is taken at  $t_k = (k-1)h$  for  $k = 1, \dots, K$ , where  $h = 0.01$  and  $K = 201$ , and the observation noise variance is set to  $\Gamma = \text{diag}(0.1, 0.01, 0.01)$ . Note that similar results were obtained for other settings of  $\Gamma$ . For the ODE solver  $\tilde{x}_k(\theta)$ , we employ the explicit Euler method with step size  $\Delta t = 1.0 \times 10^{-2}$ ,  $5.0 \times 10^{-4}$ , or  $1.0 \times 10^{-4}$ .

**4.1.1. Estimation accuracy.** First, we check the estimation accuracy of the IRLS algorithms.

Figure 4.1 plots the objective function  $g(\theta^{(l)}, w^{(l)})$  in (3.9) and squared error  $\|\hat{\theta}^{(l)} - \theta\|^2$  with respect to the iteration count  $l$  for different step sizes. The initial guess was set to  $\theta^{(0)} = [-9, -1.5, 39]^\top$ . The IRLS algorithms converge within 10 iterations, and the estimation accuracy is better for smaller step size.

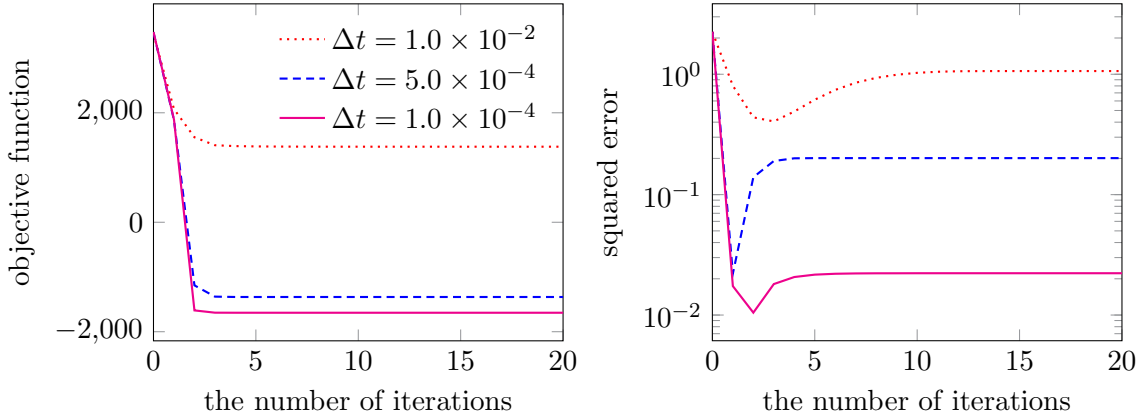


**Figure 4.1.** Plots of the objective function  $g(\theta^{(l)}, w^{(l)})$  in (3.9) (left) and the squared error  $\|\hat{\theta}^{(l)} - \theta\|^2$  (right) of IRLS (Algorithm 3.1) with three different step sizes for the Lorenz system.

Figure 4.2 plots the estimated weights  $w_{k,j}^{(20)}$  at the 20th iteration for different step sizes. Note that, from (3.7), the weight  $w_{k,j}$  does not exceed  $1/\gamma_j^2$ , which is 10 for  $j = 1$  and 100 for

$j = 2, 3$ . The estimated weights tend to be larger for smaller step sizes, which implies that the numerical solution is more reliable. In particular, the weights  $w_{k,1}^{(20)}$  for  $x_1$  are constant when  $\Delta t = 1.0 \times 10^{-4}$ , which indicates that the numerical solution is accurate enough compared to the observation noise. In this way, the IRLS algorithms provide information about the accuracy of the numerical solution as a byproduct.

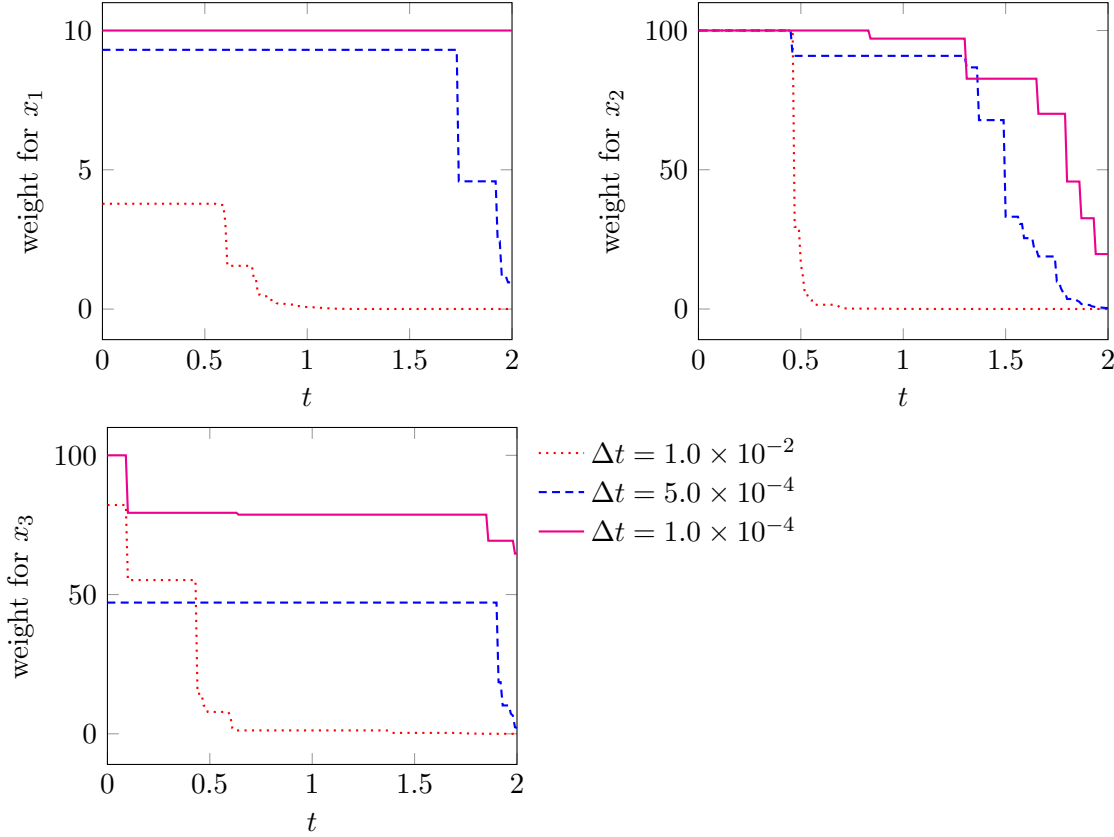


**Figure 4.2.** The estimates of weights  $w_{k,j}^{(20)}$  by IRLS(20) (Algorithm 3.2) for the Lorenz system.

Figure 4.3 compares the estimation accuracy of the IRLS algorithms with the conventional method  $\hat{\theta}_{\text{QML}}$  in (2.4), which does not account for the discretization error, for two choices of the initial guess:  $\theta^{(0)} = [-9, -1.5, 39]^\top$  and  $\theta^{(0)} = [-9.9, -0.9, 40.5]^\top$ . The IRLS algorithms have better estimation accuracy than the conventional method. In particular, the IRLS algorithms are more robust with respect to the choice of the initial guess.

**4.1.2. Discretization error quantification.** Now, we confirm that the IRLS algorithms successfully quantify the discretization error. Here, we regard the output of `ode45` with the true initial state as  $x(t; \theta)$  and fix the time step size for  $\tilde{x}(t_k; \theta)$  to  $\Delta t = 5.0 \times 10^{-4}$ .

Figure 4.4 shows the observation data  $y_1, \dots, y_K$  and the numerical solution  $\tilde{x}(t; \theta)$  with the true initial state. It implies that the discretization error  $\tilde{x}(t; \theta) - x(t; \theta)$  becomes large around  $t = 1.5$ .

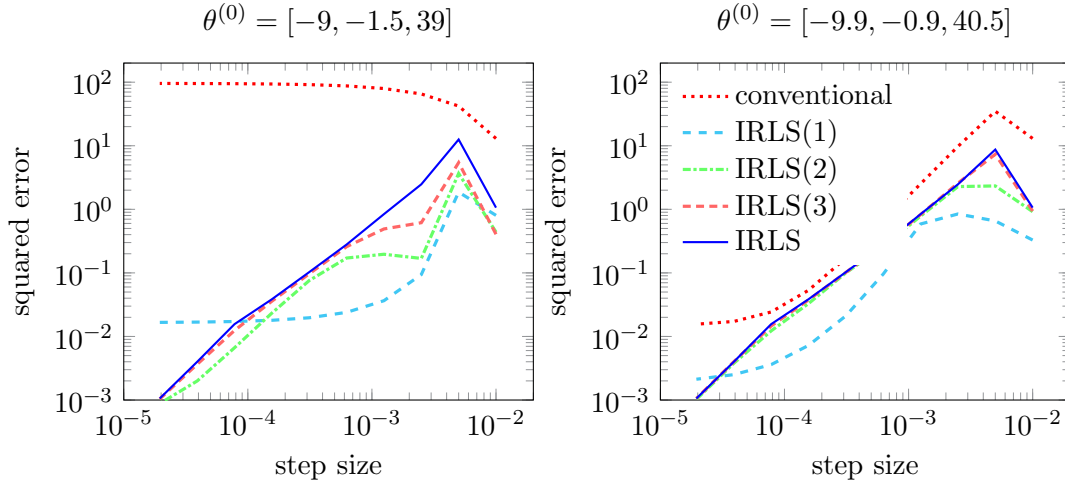


**Figure 4.3.** Comparison of squared errors of IRLS( $L$ ) (Algorithm 3.2) with several values of  $L$  and the conventional method in (2.4) for the Lorenz system. Left:  $\theta^{(0)} = [-9, -1.5, 39]^T$ . Right:  $\theta^{(0)} = [-9.9, -0.9, 40.5]^T$ .

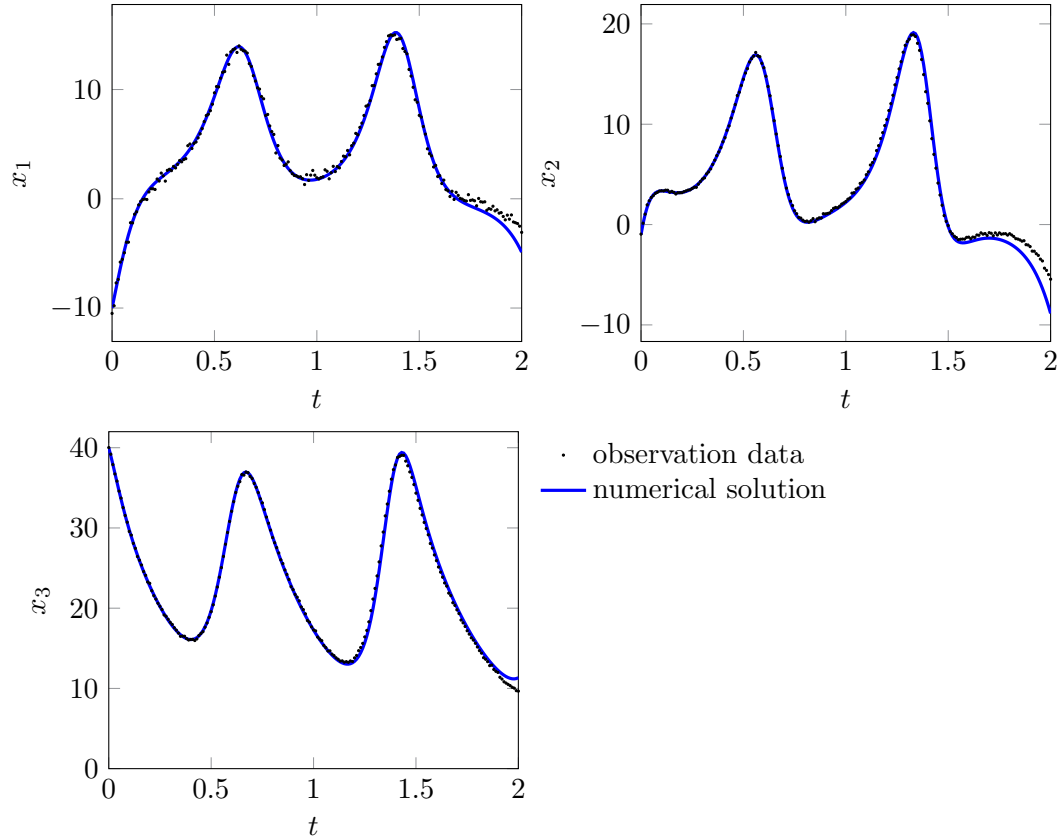


**Figure 4.4.** The observation data  $y_1, \dots, y_K$  and the numerical solution  $\tilde{x}(t; \theta)$  with step size  $\Delta t = 5.0 \times 10^{-4}$  for the Lorenz system.

Figure 4.5 plots the estimated weights  $\hat{w}_{k,j}$ , the square root of the estimated discretization error variance  $\hat{\sigma}_{k,j}$ , and the actual discretization error  $|x_j(t_k; \theta) - \tilde{x}_j(t_k; \theta)|$  for each  $j$ . The estimates of discretization error variance quantify the actual discretization error well. In particular, the actual discretization error grows rapidly after  $t = 1.5$  and this behavior is well reproduced by the estimates of discretization error variance.

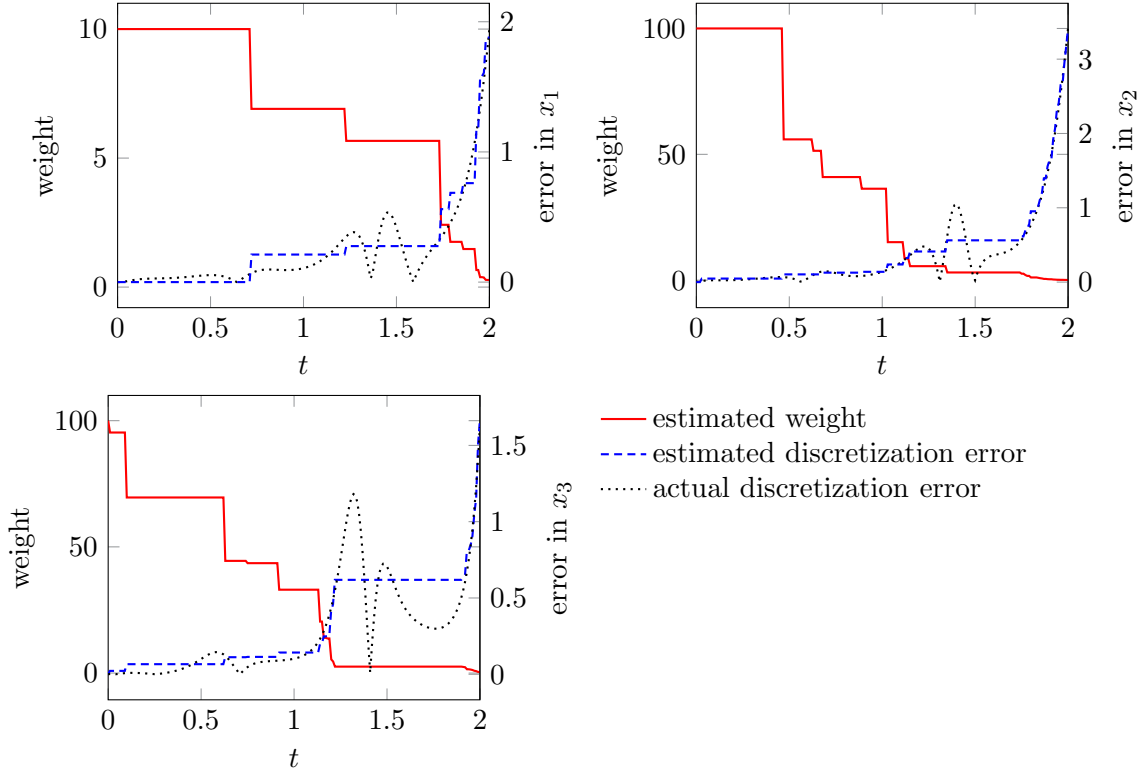


**Figure 4.5.** Estimates of weights  $\hat{w}_{k,j}$ , the estimated discretization error, i.e., the square root of the estimated observation error variance  $\hat{\sigma}_{k,j}$ , and the actual discretization error  $|x_j(t_k; \theta) - \tilde{x}_j(t_k; \theta)|$  for the Lorenz system.

**4.2. FitzHugh–Nagumo model.** Here, we consider the FitzHugh–Nagumo model [9, 20]:

$$\frac{d}{dt} \begin{bmatrix} V \\ R \end{bmatrix} = \begin{bmatrix} c \left( V - \frac{V^3}{3} + R \right) \\ -\frac{1}{c}(V - a + bR) \end{bmatrix}, \quad \begin{bmatrix} V(0) \\ R(0) \end{bmatrix} = \begin{bmatrix} -1 \\ -1 \end{bmatrix}.$$

We consider estimation of the system parameter  $\theta = [a, b, c] = [0.2, 0.2, 3]$  from the observation of  $V$ . Namely, the observation matrix  $H$  in (2.2) is  $H = [1, 0]$ . The observation is taken at  $t_k = (k-1)h$  for  $k = 1, \dots, K$ , where  $h = 0.2$  and  $K = 201$ , and the observation noise variance is set to  $\Gamma = 0.01$ .

Figure 4.6 shows the results for different step sizes  $\Delta t = 0.2, 0.01$  and the estimated

weights for the variable  $V$ . The initial guess was set to  $\theta^{(0)} = [1, 1, 1]$ . Similarly to the Lorenz system, estimation accuracy is better for smaller step sizes.

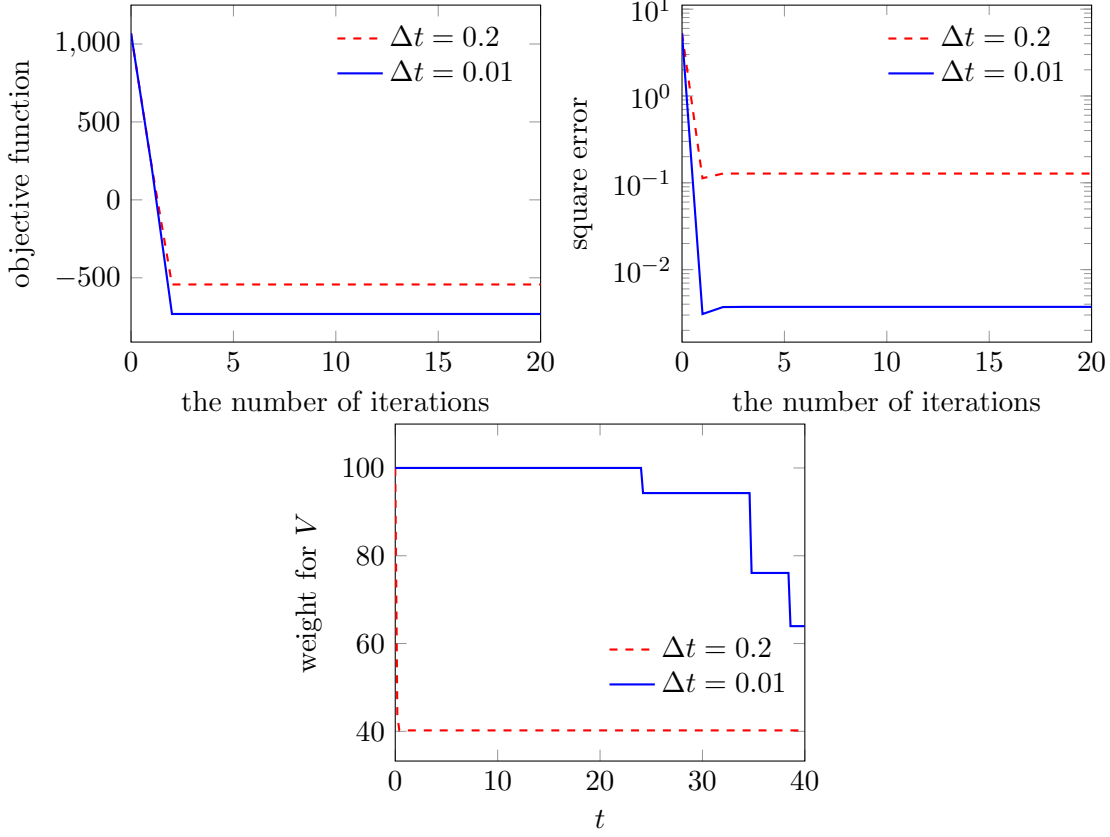


**Figure 4.6.** Plots of the objective function  $g(\theta^{(l)}, w^{(l)})$  in (3.9) (top left), the squared error  $\|\theta^{(l)} - \theta\|^2$  (top right) and the estimated weights  $w_{k,j}^{(20)}$  after 20 iterations (bottom) of IRLS (Algorithm 3.1) with two different step sizes for the FitzHugh–Nagumo model.

Figure 4.7 compares the results of IRLS( $L$ ) with the conventional method. IRLS algorithms have better estimation accuracy when the step sizes are smaller than  $10^{-2}$ , whereas both methods attain almost the same estimation accuracy for relatively large step sizes. Since the plots for IRLS(2), IRLS(3) and IRLS almost overlap each other, IRLS algorithms are considered to converge in two iterations.

**4.3. Kepler equation.** Finally, we consider the Kepler equation:

$$\frac{d}{dt} \begin{bmatrix} q_1 \\ q_2 \\ p_1 \\ p_2 \end{bmatrix} = \begin{bmatrix} p_1 \\ p_2 \\ -\frac{q_1}{(q_1^2 + q_2^2)^{3/2}} \\ -\frac{q_2}{(q_1^2 + q_2^2)^{3/2}} \end{bmatrix}, \quad \begin{bmatrix} q_1(0) \\ q_2(0) \\ p_1(0) \\ p_2(0) \end{bmatrix} = \theta.$$

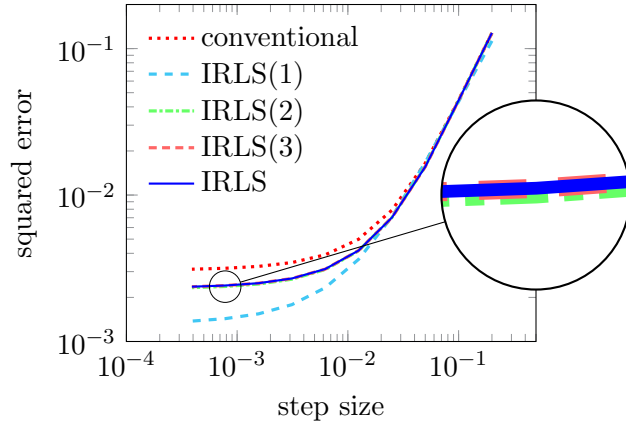


**Figure 4.7.** Comparison of the squared error of the IRLS( $L$ ) (Algorithm 3.2) with several values of  $L$  and the conventional method in (2.4) for the FitzHugh–Nagumo model. The plots for IRLS(2), IRLS(3), IRLS almost overlap each other.

We consider estimation of the initial state  $\theta = [1-e, 0, 0, \sqrt{(1+e)/(1-e)}]^\top = [0.4, 0, 0, 2]^\top$  with the eccentricity  $e = 0.6$  from the observation of  $q_1$  and  $q_2$ . Namely, the observation matrix  $H$  in (2.2) is

$$H = \begin{bmatrix} 1 & 0 & 0 & 0 \\ 0 & 1 & 0 & 0 \end{bmatrix}.$$

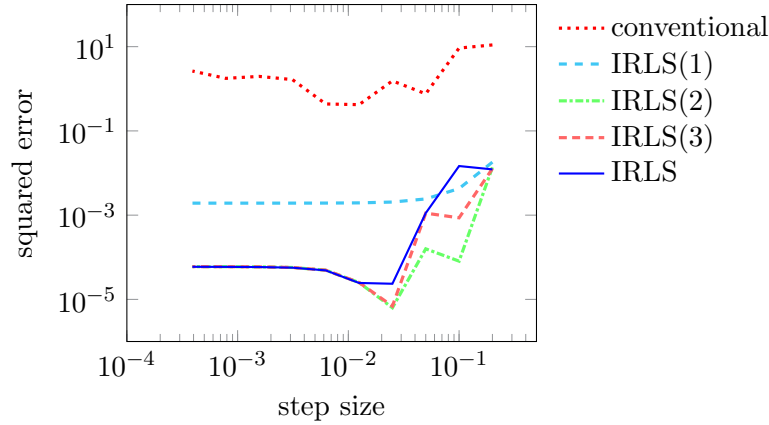
The observation is taken at  $t_k = (k-1)h$  for  $k = 1, \dots, K$ , where  $h = 0.2$  and  $K = 101$ , and the observation noise variance is set to  $\Gamma = \text{diag}(1 \times 10^{-4}, 1 \times 10^{-4})$ .

The Kepler equation is a Hamiltonian system, and symplectic integrators are often employed for solving Hamiltonian systems in practical computations [11]. Thus, we use the Störmer–Verlet method for the numerical solution  $\tilde{x}(t; \theta)$  (see Appendix C for details).

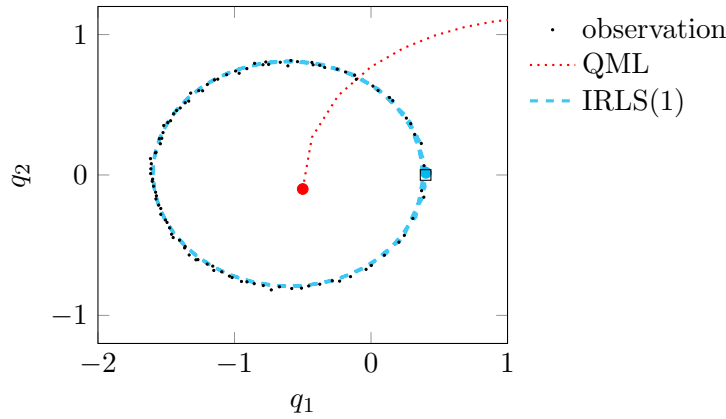
Figure 4.8 plots the squared error of the IRLS algorithms and the conventional method with respect to the step size. We set the initial guess to  $\theta^{(0)} = [0.5, 0.05, -0.05, 2.5]^\top$ . Similar to the left figure in Figure 4.3, the IRLS algorithms have better estimation accuracy than the conventional method, even with a single iteration ( $L = 1$ ).

Figure 4.9 shows the numerical solution of the Störmer–Verlet method with the initial state set to the estimate of IRLS(1) or the conventional method. The trajectory from the estimate of IRLS(1) is fairly close to the observations and well exhibit the elliptic orbit, whereas the one from the estimate of the conventional method does not reproduce the elliptic orbit.

**5. Concluding remarks.** In this paper, we developed a method for estimating ODE models that quantifies the discretization error in a data-driven manner. By modeling the discretization error as random variables, the proposed method alternately updates the discretization error variance and the ODE parameter. The isotonic regression algorithm [3, 22, 30] is employed for the update of the discretization error variance, whereas the adjoint system and symplectic partitioned Runge–Kutta method [24] are used for the update of the ODE parameter. Experimental results on several ODE models demonstrated that the proposed method improves estimation accuracy by successfully quantifying the discretization error based on



**Figure 4.8.** Comparison of the squared errors of  $\text{IRLS}(L)$  (Algorithm 3.2) with several values of  $L$  and the conventional method in (2.4) for the Kepler equation.



**Figure 4.9.** Numerical solutions of the Störmer-Verlet method (step size  $\Delta t = 0.02$ ) with the initial state set to the estimate of  $\text{IRLS}(1)$  and the conventional method in (2.4) for the Kepler equation. The true initial state is indicated by the square mark.

data. Since the proposed method converged in a few iterations in most cases, even one or two iterations is expected to provide better estimate than the conventional method in practice.

We point out several directions for future work. First, although we assumed that the observation noise variance is given, it is important to eliminate this assumption and develop a method for estimating the observation noise variance. Next, while we modeled the discretization error by random variables and assumed these random variables to be independent, this assumption may not be suitable in some cases. For example, for an ODE system with almost periodic orbit, the discretization error is also considered to be almost periodic. Thus, it is important to extend the IRLS algorithms to account for the dependence between discretization error at different time points. Finally, it is an interesting problem from the viewpoint of numerical analysis to investigate the behavior of the estimates of discretization error variance



theoretically.

### Appendix A. Proof of Theorem 3.2.

We prove the following more general statement, of which Theorem 3.2 is a special case.

**Theorem A.1.** *Let  $\hat{\nu} = (\hat{\nu}_1, \dots, \hat{\nu}_K)$  be the optimal solution of the minimization problem*

$$(A.1) \quad \min_{\nu_1 \leq \dots \leq \nu_K} \sum_{k=1}^K (\Phi(\nu_k) - \nu_k s_k),$$

where  $\Phi$  is a strictly convex function. Then, the optimal solution  $\hat{\mu} = (\hat{\mu}_1, \dots, \hat{\mu}_K)$  of the minimization problem

$$(A.2) \quad \min_{\alpha \leq \mu_1 \leq \dots \leq \mu_K} \sum_{k=1}^K (\Phi(\mu_k) - \mu_k s_k)$$

is given by  $\hat{\mu}_k = \max(\hat{\nu}_k, \alpha)$ .

The Lagrangian function for (A.1) is given by

$$L(\nu, \eta) = \sum_{k=1}^K (\Phi(\nu_k) - \nu_k s_k) + \sum_{k=1}^{K-1} \eta_k (\nu_k - \nu_{k+1}).$$

The optimal solution  $\hat{\nu}$  and its corresponding multiplier  $\hat{\eta}$  satisfy the KKT condition [4]:

$$(A.3) \quad \left. \frac{\partial F}{\partial \nu_k} \right|_{\nu=\hat{\nu}, \eta=\hat{\eta}} = \Phi'(\hat{\nu}_k) - s_k + \hat{\eta}_k - \hat{\eta}_{k-1} = 0, \quad k = 1, \dots, K,$$

where  $\hat{\eta}_0 = \hat{\eta}_K = 0$ , and

$$(A.4) \quad \hat{\eta}_k \geq 0, \quad \hat{\nu}_k - \hat{\nu}_{k+1} \leq 0, \quad \hat{\eta}_k (\hat{\nu}_k - \hat{\nu}_{k+1}) = 0, \quad k = 1, \dots, K-1.$$

Similarly, the Lagrangian function for (A.2) is defined as

$$L(\mu, \lambda) = \sum_{k=1}^K (\Phi(\mu_k) - \mu_k s_k) + \sum_{k=0}^{K-1} \lambda_k (\mu_k - \mu_{k+1}),$$

where  $\mu_0 = \alpha$ . The KKT condition for the optimal solution  $\hat{\mu}$  and its corresponding multiplier  $\hat{\lambda}$  is given by

$$(A.5) \quad \left. \frac{\partial F}{\partial \mu_k} \right|_{\mu=\hat{\mu}, \lambda=\hat{\lambda}} = \Phi'(\hat{\mu}_k) - s_k + \hat{\lambda}_k - \hat{\lambda}_{k-1} = 0, \quad k = 1, \dots, K,$$

where  $\hat{\nu}_K = 0$ , and

$$(A.6) \quad \hat{\lambda}_k \geq 0, \quad \hat{\mu}_k - \hat{\mu}_{k+1} \leq 0, \quad \hat{\lambda}_k (\hat{\mu}_k - \hat{\mu}_{k+1}) = 0, \quad k = 0, \dots, K-1,$$

where  $\hat{\mu}_0 = \alpha$ . Note that the KKT condition (A.5) and (A.6) is not only necessary but also sufficient for the optimality of  $\hat{\mu}$ , since both the objective function and feasible region are convex [4].

Without loss of generality, assume

$$\hat{\nu}_1 \leq \cdots \leq \hat{\nu}_{K'} < \alpha \leq \hat{\nu}_{K'+1} \leq \cdots \leq \hat{\nu}_K.$$

Let  $\hat{\mu}_k = \alpha$  for  $k = 1, \dots, K'$  and  $\hat{\mu}_k = \hat{\nu}_k$  for  $k = K' + 1, \dots, K$ . Also, let  $\hat{\lambda}_k = \hat{\eta}_k$  for  $k = K', \dots, K - 1$  and define  $\hat{\lambda}_{K'-1}, \dots, \hat{\lambda}_0$  backwardly by  $\hat{\lambda}_k = \Phi'(\hat{\mu}_{k+1}) - s_{k+1} + \hat{\lambda}_{k+1}$ . We show that  $(\hat{\mu}, \hat{\lambda})$  satisfies (A.5) and (A.6), which completes the proof.

First, from  $\hat{\lambda}_k = \Phi'(\hat{\mu}_{k+1}) - s_{k+1} + \hat{\lambda}_{k+1}$  for  $k = 0, \dots, K' - 1$ , the condition (A.5) is satisfied for  $k = 1, \dots, K'$ . Also, since  $\hat{\mu}_k = \hat{\nu}_k$  and  $\hat{\lambda}_k = \hat{\eta}_k$  for  $k = K' + 1, \dots, K$  and (A.3) holds, the condition (A.5) is satisfied for  $k = K' + 1, \dots, K$ .

From the third condition in (A.4) for  $k = K'$  and the assumption  $\hat{\nu}_{K'} < \hat{\nu}_{K'+1}$ , we have  $\hat{\lambda}_{K'} = \hat{\eta}_{K'} = 0$ . Since  $\Phi$  is strictly convex,

$$\hat{\lambda}_{K'-1} = \Phi'(\hat{\mu}_{K'}) - s_{K'} + \hat{\lambda}_{K'} \geq \Phi'(\hat{\nu}_{K'}) - s_{K'} + \hat{\eta}_{K'} = \hat{\eta}_{K'-1}.$$

By induction, we have  $\hat{\lambda}_k \geq \hat{\eta}_k$  for  $k = 0, \dots, K' - 1$ . Thus, from the first condition in (A.4), the first condition in (A.6) is satisfied for  $k = 0, \dots, K' - 1$ . Also, from  $\hat{\lambda}_k = \hat{\eta}_k$  for  $k = K', \dots, K - 1$ , the first condition in (A.6) is satisfied for  $k = K', \dots, K - 1$ .

From the definition of  $\hat{\mu}$ , the second condition in (A.6) is satisfied for  $k = 0, \dots, K - 1$ .

Finally, from  $\hat{\lambda}_{K'} = 0$  and  $\hat{\mu}_k = \alpha$  for  $k = 0, \dots, K'$ , the third condition in (A.6) are satisfied for  $k = 0, \dots, K'$ . In addition, from  $\hat{\mu}_k = \hat{\nu}_k$  and  $\hat{\lambda}_k = \hat{\eta}_k$  for  $k = K' + 1, \dots, K - 1$  and the third condition in (A.4), the third condition in (A.6) is also satisfied for  $k = K' + 1, \dots, K - 1$ .

## Appendix B. Geometric Integration and symplectic partitioned Runge–Kutta methods.

Geometric numerical integration methods or structure-preserving numerical methods are numerical methods that preserve or inherit the underlying geometric properties of differential equations. The main advantage of geometric numerical integration methods is that in many cases we can expect qualitatively better numerical solutions, especially over a long period of time, than general-purpose methods. For more details on this subject, see [10, 11, 17].

Consider a coupled system

$$(B.1) \quad \frac{d}{dt} \begin{bmatrix} x \\ z \end{bmatrix} = \begin{bmatrix} f_1(x, z, t) \\ f_2(x, z, t) \end{bmatrix}, \quad \begin{bmatrix} x(0) \\ z(0) \end{bmatrix} = \begin{bmatrix} x_0 \\ z_0 \end{bmatrix},$$

where  $x \in \mathbb{R}^{M_1}$  and  $z \in \mathbb{R}^{M_2}$  are time-dependent vectors and  $f_1 : \mathbb{R}^{M_1} \times \mathbb{R}^{M_2} \times \mathbb{R} \rightarrow \mathbb{R}^{M_1}$ ,  $f_2 : \mathbb{R}^{M_1} \times \mathbb{R}^{M_2} \times \mathbb{R} \rightarrow \mathbb{R}^{M_2}$ . A partitioned Runge–Kutta (PRK) method applied to (B.1) reads

$$x_{n+1} = x_n + \Delta t_n \sum_{i=1}^s b_i k_{n,i}, \quad z_{n+1} = z_n + \Delta t_n \sum_{i=1}^s B_i l_{n,i},$$

where

$$k_{n,i} = f_1(X_{n,i}, Z_{n,i}, t_n + c_i \Delta t_n), \quad l_{n,i} = f_2(X_{n,i}, Z_{n,i}, t_n + C_i \Delta t_n),$$

and the internal stages  $X_{n,i}, Z_{n,i}$  for  $i = 1, \dots, s$  are defined by

$$X_{n,i} = x_n + \Delta t_n \sum_{j=1}^s a_{ij} k_{n,j}, \quad Z_{n,i} = z_n + \Delta t_n \sum_{j=1}^s A_{ij} k_{n,j}.$$

Note that in this appendix  $t_n$  does not mean the time points the observations are made, but it simply means the time grid of the numerical method:  $t_{n+1} - t_n = \Delta t_n$ .

It is known that a PRK method preserves certain quadratic invariants if the coefficients of the method satisfies a certain condition. More precisely, the following theorem holds.

**Theorem B.1** (e.g. [11, Chapter IV, Theorem 2.4], [24, Theorem 2.4]). *Assume that  $S : \mathbb{R}^{M_1} \times \mathbb{R}^{M_2} \rightarrow \mathbb{R}$  is a real valued bilinear map, and the solution to (B.1) satisfies*

$$\frac{d}{dt} S(x(t), z(t)) = 0.$$

*If the PRK coefficients satisfy*

$$(B.2) \quad b_i = B_i, \quad i = 1, \dots, s, \quad b_i A_{ij} + B_j a_{ji} = b_i B_i, \quad i, j = 1, \dots, s$$

*and*

$$(B.3) \quad c_i = C_i, \quad i = 1, \dots, s,$$

*it follows that for the solution to the PRK method  $S(x_n, z_n)$  is constant, i.e. it is independent of  $n$ .*

A PRK method is called a symplectic PRK method if its coefficients satisfy (B.2), because such a PRK method exactly preserves the symplecticity when applied to Hamiltonian systems [11].

The key idea to obtaining the exact gradient in Section 3.4 is to couple the original system (3.15) and the adjoint system, and to apply a symplectic PRK method (precisely speaking, the variational equations  $\dot{\delta} = \nabla_x f(x) \delta$  should be taken into account, but we omit the detail since in practice there is no need to integrate the variational equations). For example, when  $s = 1$ , if the original system is integrated by using the explicit Euler method (3.17), i.e.  $(a, b, c) = (1, 1, 1)$ , then the adjoint system should be solved by the method  $(A, B, C) = (0, 1, 1)$  so that the pairs of the coefficients satisfy the conditions (B.2) and (B.3). The choice  $(A, B, C) = (0, 1, 1)$  leads to the scheme (3.18).

### Appendix C. The Störmer–Verlet method.

The Störmer–Verlet method is a typical symplectic partitioned Runge–Kutta method [11]. It has been widely used to integrate Hamiltonian systems, especially those from celestial mechanics and molecular dynamics. We employ the Störmer–Verlet method to integrate the Kepler equation in Section 4.3.

In general, for a system of ODEs of the form

$$(C.1) \quad \frac{d}{dt} \begin{bmatrix} q \\ p \end{bmatrix} = \begin{bmatrix} p \\ -f(q) \end{bmatrix},$$

the one step formula  $(\tilde{q}_n, \tilde{p}_n) \mapsto (\tilde{q}_{n+1}, \tilde{p}_{n+1})$  of the Störmer–Verlet method is defined by

$$\begin{aligned}\tilde{q}_{n+1/2} &= \tilde{q}_n + \frac{\Delta t_n}{2} \tilde{p}_n, \\ \tilde{p}_{n+1} &= \tilde{p}_n - \Delta t_n f(\tilde{q}_{n+1/2}), \\ \tilde{q}_{n+1} &= \tilde{q}_{n+1/2} + \frac{\Delta t_n}{2} \tilde{p}_{n+1},\end{aligned}$$

where  $\Delta t_n$  is the time step size.

The adjoint system (3.16) for (C.1) is

$$(C.2) \quad \frac{d}{dt} \begin{bmatrix} \lambda \\ \nu \end{bmatrix} = \begin{bmatrix} \nabla_q f(q)^\top \nu \\ -\lambda \end{bmatrix}.$$

To obtain the exact gradient defined with the numerical solutions of the Störmer–Verlet method, we need to follow the discussion in Appendix B. But the difficulty is that while in Appendix B (and [24]) the original equation is assumed to be solved by a standard Runge–Kutta method, in this case the original equation is solved by the PRK method. It turns out that the discussion in Appendix B can be extended to the case that the original equation itself is solved by a PRK method. To obtain the exact gradient defined with the numerical solutions of the Störmer–Verlet method, the adjoint system (C.2) should be numerically integrated backwardly by the formula

$$\begin{aligned}\tilde{\nu}_{n+1/2} &= \tilde{\nu}_n - \frac{\Delta t_n}{2} \tilde{\lambda}_n \\ \tilde{\lambda}_{n+1} &= \tilde{\lambda}_n + \Delta t_n \nabla_q f(\tilde{q}_{n+1/2})^\top \tilde{\nu}_{n+1/2}, \\ \tilde{\nu}_{n+1} &= \tilde{\nu}_{n+1/2} - \frac{\Delta t_n}{2} \tilde{\lambda}_{n+1}.\end{aligned}$$

## REFERENCES

- [1] A. ABDULLE AND G. GAREGNANI, *Random time step probabilistic methods for uncertainty quantification in chaotic and geometric numerical integration*, 2018, <https://arxiv.org/abs/arXiv:1801.01340>.
- [2] A. ARNOLD, D. CALVETTI, AND E. SOMERSALO, *Linear multistep methods, particle filtering and sequential Monte Carlo*, *Inverse Problems*, 29 (2013), pp. 085007, 25, <https://doi.org/10.1088/0266-5611/29/8/085007>.
- [3] R. E. BARLOW, D. J. BARTHOLOMEW, J. M. BREMNER, AND H. D. BRUNK, *Statistical Inference Under Order Restrictions. The Theory and Application of Isotonic Regression*, John Wiley & Sons, London-New York-Sydney, 1972.
- [4] S. BOYD AND L. VANDENBERGHE, *Convex Optimization*, Cambridge University Press, 2004.
- [5] J. C. BUTCHER, *Numerical Methods for Ordinary Differential Equations*, John Wiley & Sons, Ltd., Chichester, third ed., 2016.
- [6] O. A. CHKREBTHI, D. A. CAMPBELL, B. CALDERHEAD, AND M. A. GIROLAMI, *Bayesian solution uncertainty quantification for differential equations*, *Bayesian Anal.*, 11 (2016), pp. 1239–1267, <https://doi.org/10.1214/16-BA1017>.
- [7] J. COCKAYNE, C. J. OATES, T. SULLIVAN, AND M. GIROLAMI, *Bayesian probabilistic numerical methods*, to appear in *SIAM Rev.*
- [8] P. R. CONRAD, M. GIROLAMI, S. SÄRKKÄ, A. STUART, AND K. ZYGALAKIS, *Statistical analysis of differential equations: introducing probability measures on numerical solutions*, *Stat. Comput.*, 27 (2017), pp. 1065–1082, <https://doi.org/10.1007/s11222-016-9671-0>.

- [9] R. FITZHUGH, *Impulses and physiological states in models of nerve membrane*, Biophys. J., 1 (1961), pp. 445–466, [https://doi.org/10.1016/S0006-3495\(61\)86902-6](https://doi.org/10.1016/S0006-3495(61)86902-6).
- [10] E. HAIRER, C. LUBICH, AND G. WANNER, *Geometric numerical integration illustrated by the Störmer–Verlet method*, Acta Numer., 12 (2003), pp. 399–450, <https://doi.org/10.1017/S0962492902000144>.
- [11] E. HAIRER, C. LUBICH, AND G. WANNER, *Geometric Numerical Integration: Structure-Preserving Algorithms for Ordinary Differential equations*, Springer-Verlag, Berlin, second ed., 2006.
- [12] E. HAIRER, R. I. McLACHLAN, AND A. RAZAKARIVONY, *Achieving Brouwer’s law with implicit Runge–Kutta methods*, BIT, 48 (2008), pp. 231–243, <https://doi.org/10.1007/s10543-008-0170-3>.
- [13] E. HAIRER, S. P. NØRSETT, AND G. WANNER, *Solving Ordinary Differential Equations I. Nonstiff Problems*, Springer-Verlag, Berlin, second ed., 1993.
- [14] P. HENNIG AND S. HAUBERG, *Probabilistic solutions to differential equations and their application to Riemannian statistics*, in Artificial Intelligence and Statistics, 2014, pp. 347–355.
- [15] P. HENNIG, M. A. OSBORNE, AND M. GIROLAMI, *Probabilistic numerics and uncertainty in computations*, Proc. R. Soc. Lond. Ser. A Math. Phys. Eng. Sci., 471 (2015), p. 20150142, <https://doi.org/10.1098/rspa.2015.0142>.
- [16] H. KERSTING AND P. HENNIG, *Active uncertainty calibration in Bayesian ODE solvers*, in Uncertainty in Artificial Intelligence, 2016, pp. 309–318.
- [17] B. LEIMKUHLER AND S. REICH, *Simulating Hamiltonian Dynamics*, Cambridge University Press, Cambridge, 2004.
- [18] H. C. LIE, T. J. SULLIVAN, AND A. STUART, *Strong convergence rates of probabilistic integrators for ordinary differential equations*, to appear in Stat. Comput.
- [19] E. N. LORENZ, *Deterministic nonperiodic flow*, J. Atmos. Sci., 20 (1963), pp. 130–141, [https://doi.org/10.1175/1520-0469\(1963\)020<0130:DNF>2.0.CO;2](https://doi.org/10.1175/1520-0469(1963)020<0130:DNF>2.0.CO;2).
- [20] J. S. NAGUMO, S. ARIMOTO, AND S. YOSHIZAWA, *An active pulse transmission line simulating a nerve axon*, Proc. Inst. Radio Engrs, 50 (1962), pp. 2061–2070, <https://doi.org/10.1109/JRPROC.1962.288235>.
- [21] C. J. OATES, J. COCKAYNE, R. G. AYKROYD, AND M. GIROLAMI, *Bayesian probabilistic numerical methods in time-dependent state estimation for industrial hydrocyclone equipment*, to appear in J. Am. Stat. Assoc.
- [22] T. ROBERTSON, F. T. WRIGHT, AND R. L. DYKSTRA, *Order Restricted Statistical Inference*, Wiley Series in Probability and Mathematical Statistics: Probability and Mathematical Statistics, John Wiley & Sons, Ltd., Chichester, 1988.
- [23] J. M. SANZ-SERNA, *Symplectic integrators for Hamiltonian problems: an overview*, Acta Numer., 1 (1992), pp. 243–286, <https://doi.org/10.1017/s0962492900002282>.
- [24] J. M. SANZ-SERNA, *Symplectic Runge–Kutta schemes for adjoint equations, automatic differentiation, optimal control, and more*, SIAM Rev., 58 (2016), pp. 3–33, <https://doi.org/10.1137/151002769>.
- [25] J. M. SANZ-SERNA AND M. P. CALVO, *Numerical Hamiltonian Problems*, Chapman & Hall, London, 1994.
- [26] M. SCHÖBER, D. K. DUVENAUD, AND P. HENNIG, *Probabilistic ODE solvers with Runge–Kutta means*, in Advances in Neural Information Processing Systems 27, 2014, pp. 739–747.
- [27] M. SCHÖBER, S. SÄRKÄ, AND P. HENNIG, *A probabilistic model for the numerical solution of initial value problems*, Stat. Comput., 29 (2019), pp. 99–122, <https://doi.org/10.1007/s11222-017-9798-7>.
- [28] O. TEYMUR, K. ZYGALAKIS, AND B. CALDERHEAD, *Probabilistic linear multistep methods*, in Advances in Neural Information Processing Systems 29, 2016, pp. 4314–4321.
- [29] F. TRONARP, H. KERSTING, S. SÄRKÄ, AND P. HENNIG, *Probabilistic solutions to ordinary differential equations as non-linear Bayesian filtering: A new perspective*, 2018, <https://arxiv.org/abs/arXiv:1810.03440>.
- [30] C. VAN EEDEN, *Restricted Parameter Space Estimation Problems*, Springer, New York, 2006, <https://doi.org/10.1007/978-0-387-48809-7>.